ISSN 1990-7931, Russian Journal of Physical Chemistry B, 2023, Vol. 17, No. 6, pp. 1361–1369. © Pleiades Publishing, Ltd., 2023.
Russian Text © The Author(s), 2023, published in Khimicheskaya Fizika, 2023, Vol. 42, No. 11, pp. 54–62.

CHEMICAL PHYSICS OF POLYMER MATERIALS

Magnetic Resonance Imaging Study of Water Absorption of Polymer Composite Materials Subjected to Mechanical and Temperature Impact

E. V. Morozov[a, b, *], A. V. Il'ichev[a], and V. M. Bouznik[a]

[a] *Kirensky Institute of Physics of the Siberian Branch of the Russian Academy of Sciences, Krasnoyarsk, Russia*
[b] *Institute of Chemistry and Chemical Technology of the Siberian Branch of the Russian Academy of Sciences, Krasnoyarsk, Russia*
**e-mail: morozovev@iph.krasn.ru*

Received February 5, 2023; revised April 11, 2023; accepted April 20, 2023

Abstract—The results of a study of water absorption processes by samples of polymer composite materials (PCMs) based on fiberglass, subjected to low-speed impact with controlled impact energy and alternating temperature cycling are presented. Using magnetic resonance imaging (MRI), the distribution of absorbed water in the fiberglass structure is visualized and the dynamics of its accumulation in various areas of the sample are studied. It is found that mechanical impact leads to a nonuniform distribution of the absorbed water in the samples and a significant accumulation of free water in the areas of destruction and adjacent layers in the event of a violation of the integrity of the outer layer of the material. It is shown that cyclic alternating temperature effects do not lead to a noticeable change in the water absorption processes and are comparable in effect to mechanical nondestructive impacts. The results obtained using MRI are in close agreement with the data of traditional weight measurements, which shows the effectiveness of the method in diagnosing defects and mechanical damage to PCMs exposed to the humid environment.

Keywords: composite material, fiberglass, nuclear magnetic resonance, magnetic resonance imaging, water absorption

DOI: 10.1134/S1990793123060064

1. INTRODUCTION

Interest in composite materials in the world is steadily growing, as an increasing number of structures and products previously made from metal are beginning to be produced from polymer composite materials (PCMs), which have a wide range of useful properties that can easily be varied to suit operational requirements [1]. The use of PCMs makes it possible to design products with higher technological and operational capabilities, which is important in the automotive, aerospace, and aviation industries, where, of course, the most important role is played by indicators such as the material's weight, good physical and mechanical characteristics, radio transparency, corrosion resistance, etc.

Despite all their advantages, PCMs also have limitations. In particular, they cannot be classified as hydrophobic materials, and the presence of water in them not only changes their properties, including performance, but can also contribute to the premature destruction of PCMs. PCMs vary in their ability to absorb water depending on the nature of the reinforcing filler (carbon, glass, aramid, basalt, cellulose, etc. [2, 3]) and the chemical composition of the polymer matrix (organosilicon, epoxy, phenol-formaldehyde, etc. [4]). In addition, for matrices, the influence of modifying components on water diffusion and additional factors should be taken into account: the introduction of plasticizers, coloring compounds, reinforcing fillers, etc. The average level of moisture absorption when the equilibrium state reaches a plateau for PCMs is as follows: carbon fiber plastic, 0.5–1%; fiberglass, 1–2%; and organoplastics, 1.5–5%. However, even seemingly low water absorption rates greatly affect the physical and mechanical characteristics of PCMs, reducing them by an average of 15–25% (depending on the composition of the material). In relation to this, determining the ability of PCMs to absorb water is an important step in their development and implementation in industrial practice.

The most used methods for determining the moisture content in PCMs are (1) measurement of the mass of samples during the process of sorption and desorption of water; (2) full-scale exposure of materials by preliminary and subsequent drying of samples until the mass stabilizes; (3) analytical method of Fischer titration using gas chromatography and Fourier transform infrared spectroscopy [5]. The first two

methods are simple in technical terms and provide information about the mass of water absorbed and desorbed in the sample; the third method allows us to determine the type of water (bound, free). The most accessible weight methods are integral: they characterize the sample as a whole and do not give an idea of the nature of the distribution of water in the volume of the sample, which is extremely important, especially if there are defects in the PCM sample that appear when the technological conditions of sample manufacturing or external mechanical influence are violated. Thus, the use of new methods that can provide information about the state and localization of water inside the test sample is an urgent task. An effective method that can provide such information is magnetic resonance imaging (MRI). This method has received widespread recognition in the field of medical diagnostics and research of biological systems [6], but its application in the field of materials science is quite limited [7, 8]. Despite this, a number of studies have demonstrated the effectiveness of MRI in studying the processes of water absorption and swelling in polymer and composite materials [9–11].

In this paper, the MRI method was applied to study the processes of water absorption by a PCM based on an epoxy binder and woven glass filler. The water absorption by fiberglass was analyzed after two preliminary impacts simulating operational factors. The first factor is mechanical damage, which for a real structure can be caused by a complex stress state or external influence (for example, an impact). The second factor is climatic influence: operation under cyclic exposure to alternating temperatures, exposure to a hot and humid environment, thermal cycling, etc. These factors can manifest themselves separately and together, contributing to the accumulation of micro- and macrostructural damage in the material and significantly increasing water absorption, as a result of which the elastic-strength characteristics are reduced, up to the premature destruction of the material during operation.

2. EXPERIMENTAL

In order to carry out research, a fiberglass plate of the VPS-48 brand was manufactured (National Research Center "Kurchatov Institute" (VIAM), Russia) based on the epoxy binder brand VSE-1212 (National Research Center "Kurchatov Institute" (VIAM), Russia) and glass fabric produced by Porcher with a quasi-isotropic symmetrical reinforcement pattern $[+45; 0; 90; -45]_{24}$ according to the standard mode [12, 13]. Samples 80 mm long and 10 mm wide were then made from a 4-mm-thick slab and subjected to a low-speed impact. Samples 30 mm long and 10 mm wide were also produced, which were subsequently subjected to alternating temperature effects.

The creation of controlled defects (cracks, delaminations, etc.) in samples caused by low-speed impact was carried out using a PSd 50/15 (Germany) model pendulum impact driver with a scale of stored pendulum energy of up to 15 J. Mechanical tests were carried out using the Charpy method (GOST (State Standard) 4647-2015) to determine the impact strength of samples without a notch. The values of the parameters of the mechanical action of the pendulum on the studied samples are given in Table 1, and photographs of the corresponding samples are presented in Fig. 1. Depending on the impact energy on the samples, the nature of the local destruction area changes. As a result, during the sorption process, the areas of water distribution in the PCM structure will have a different character [14–16].

The optimal impact energies for four groups of samples were selected (Table 1): (group I, 0.5 J/mm; group II, 0.7 J/mm; group III, 1.0 J/mm; group IV, 1.3 J/mm). Groups of samples I and II did not receive visible damage after the impact. In group III, defects were observed in the form of internal interlayer delaminations (light spots), and when examined on a BX51 model Olympus microscope (Japan) with a magnification of ×50, defects (cracks) were found on the surface zone of the sample. In the samples in group IV, upon visual inspection, destruction was observed: defects in the contact zone of the striker with the sample (violation of continuity, and on the reverse side, destruction of the reinforcing filler and matrix in the form of a crack).

The second series of samples was subjected to cyclic exposure to alternating temperatures. To do this, the sample, located at room temperature, was placed in a tank with liquid nitrogen (–196°C) and kept for 7–12 minutes, then returned to its original conditions, where it was warmed up for 10–15 min. After this, the sample was thoroughly wiped to eliminate atmospheric moisture condensation. Water saturation was carried out after the end of the planned cyclic alternating temperature exposure. The following samples were used: 0, the initial sample; and 100, 350, and 1400 were the number of room temperature–liquid nitrogen temperature cycles.

After the specified exposure, the samples were placed in distilled water at room temperature (+23°C), where they were kept for 365 days. At certain time intervals, changes in the mass of the samples were recorded and tomographic images were recorded. Mass measurements were carried out using a GH 252 analytical balance manufactured by AND (Japan).

The tomographic images were recorded using an AVANCE DPX 200 NMR spectrometer manufactured by Bruker (Germany) with a tomographic attachment in the following configuration: a superconducting cryosolenoid with a warm hole with a diameter of 89 mm and a constant magnetic field of 4.7 T; the GREAT 3/60 gradient system; a MICRO 2.5 probe with the maximum magnetic field gradient amplitude of 1 T/m; and a 1H birdcage radio frequency coil with a diameter of 25 mm. Image acquisi-

Table 1. Low-speed impact results

Group	Sample no.	Energy stored by pendulum per mm of sample, J	Energy stored by pendulum based on the total thickness of the sample, J	Visual nature of destruction	Analysis of the nature of destruction under a microscope
I	2-1	0.5	2.94	No visible damage	–
	2-2	0.5	2.83		–
	2-3	0.5	2.95		–
II	2-4	0.7	4.10	No visible damage	–
	2-5	0.7	4.12		–
	2-6	0.7	3.89		–
III	2-7	1	5.56	No visible damage	–
	2-8	1	5.88	Defects in the form of internal interlayer delaminations (light spots)	Front side: defects in the form of cracks on the surface layer
	2-9	1	5.91		
IV	2-10	1.3	7.54	Defects in the contact area of the striker (discontinuity); reverse side: destruction of the reinforced filler or matrix (delamination)	Destruction of the surface layer, matrix defects, delamination across the section
	2-11	1.3	7.70		
	2-12	1.3	7.62		

tion and data processing were carried out using the ParaVision 4.0 spectrometer software.

Due to the short nuclear magnetic relaxation times of water in solid materials, tomographic images were obtained using a single point imaging (SPI) technique, which gives an integral distribution of the NMR signal intensity over the entire thickness of the selected imaging direction (Fig. 2). Image parameters: TR (pulse repetition time), 4 ms; field of view (FOV), 20 mm; matrix 32 × 32 pixels; number of acquisitions (NEX), 40; and recording time (TA), 3 min. To correctly normalize the signal within the images, the reference signal from water in a sealed capillary located in the field of view of the tomographic image was used.

3. RESULTS AND DISCUSSION

Study of Water Absorption of PCM Subjected to Impact

Figure 3 shows graphs of changes in the mass of samples depending on the time of water absorption. From these graphs it is clearly seen that the sample with a destroyed surface absorbs noticeably more water (up to 2 wt %), especially during the first 10 days after the start of the process. Apparently, this is due to the intense absorption of water, primarily by the destroyed layers [17, 18]. After this, the phase of water absorption by the remaining mass of the sample begins and the growth of the curve differs little from that for the other samples. Obviously, weight measurements do not allow us to differentiate the contribution to the total change in the mass of samples made by areas damaged as a result of exposure. For a deeper understanding of the ongoing processes, the MRI method was used.

Figure 4 shows tomograms of the control sample 2-16 and two samples after impact, 2-9 and 2-12, obtained during the process of water absorption. Since for samples of groups I and II the general appearance of the picture of the ongoing processes is practically no different from that for the control sample, they are not presented in Fig. 4. From the presented tomograms, it is clear that when the surface layers of the PCM 2-12 sample are destroyed, a significant change in the nature of water absorption is observed: rapid accumulation of water occurs in the zone of greatest destruction to a depth of up to one-third of the thickness of the sample. In this case, the most intense signal of absorbed water is detected directly in the zone of the discontinuity in the material (macrocrack), which is clearly visualized on the tomograms in the vertical plane (not presented in this study). This occurs to a greater extent due to the mobile (unbound) water during the moisture transfer in the area of defects and in the zone of the free volume of the sample formed after the impact. As shown by the weight measurements, in the case of mechanical impact that does not lead to damage to the external surface of the sample (i.e., where integrity is maintained even in the presence of internal defects in the form of interlayer delaminations), the difference in water absorption between the control and damaged samples is insignifi-

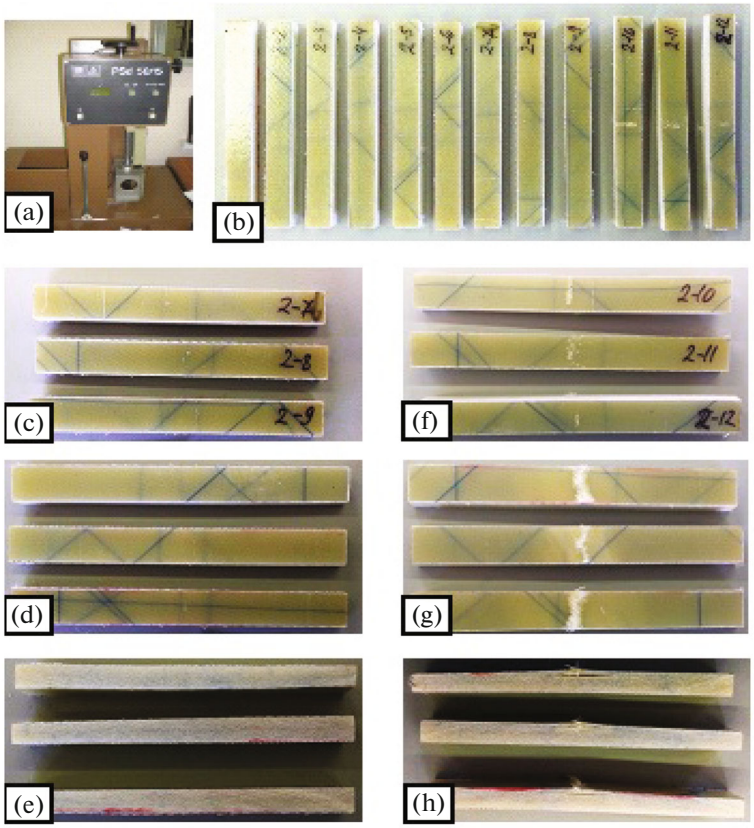

Fig. 1. PCM samples after impact. (a) pendulum pile driver; (b) general view of the samples after impact (front side); (c–e) samples of group III in three isometric planes; (f–h) samples of group IV in three isometric planes.

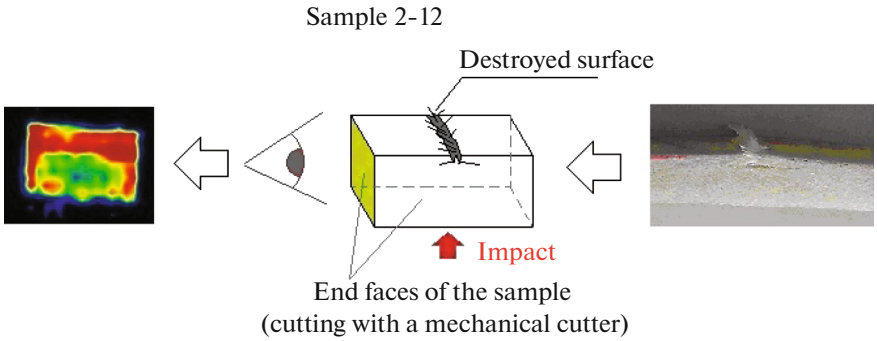

Fig. 2. Scheme of projection of tomograms relative to the sample geometry.

cant. This is consistent with the MRI imaging results, which demonstrate similar water absorption patterns between the control and mechanically stressed samples.

The signal intensity profiles in the tomograms plotted along the thickness of the sample showed a weak change in the signal with the increasing time of contact with the water for the control sample and a slightly larger variation for the damaged samples. Moreover, the difference between the last (260d) and initial (0d) profiles for each of the presented samples, normalized to the signal intensity of its initial profile, demonstrates asymmetric water absorption caused by a directed impact (Fig. 5a). Thus, for the control sample, the relative increase in the signal is approximately the same from both planes, while in the samples subjected to mechanical impact, there is a predominant accumulation of moisture from the surface with a defective structure (on the opposite side from the impact). This is especially visible in sample 2-12, one of the surfaces of which was destroyed. Integrating the

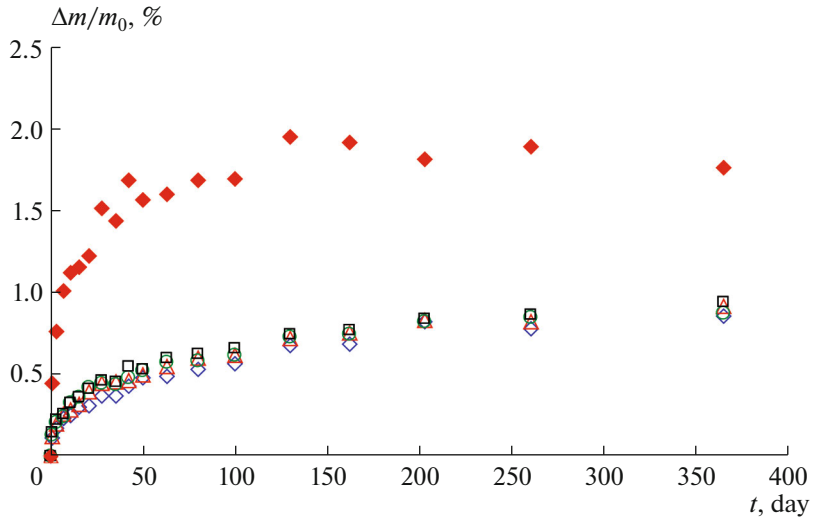

Fig. 3. Change in the mass of samples during exposure to water after mechanical impact: ◇ control sample 2-16, not exposed; △ sample 2-3; ○, sample 2-6; □, sample 2-9; ◆, sample 2-12.

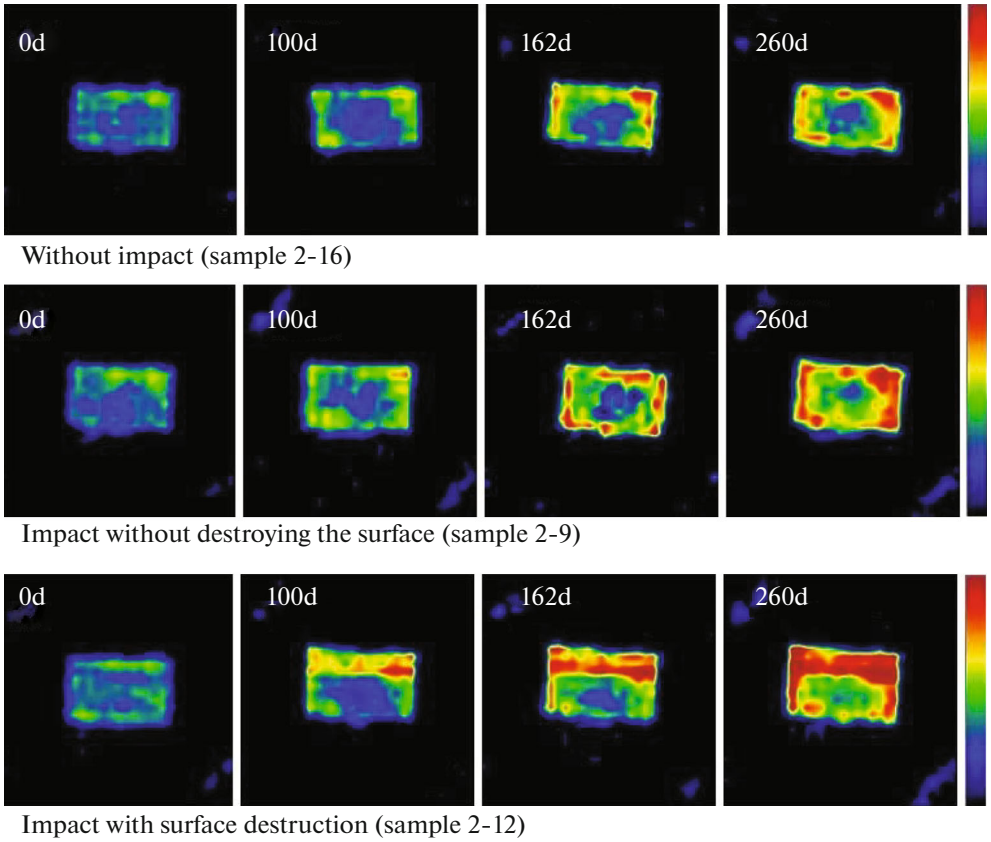

Fig. 4. Tomograms of the control (2-16) and impacted (2-9, 2-12) samples during the process of water absorption.

area under the presented curves allows us to evaluate the impact of the impact on the relative increase in signal intensity *I*. It turned out that the integral grows exponentially with increasing total impact energy (J) (Fig. 5b).

Study of Water Absorption of PCM Exposed to Temperature Impact

Weight measurements of the process of water absorption by samples exposed to the temperature

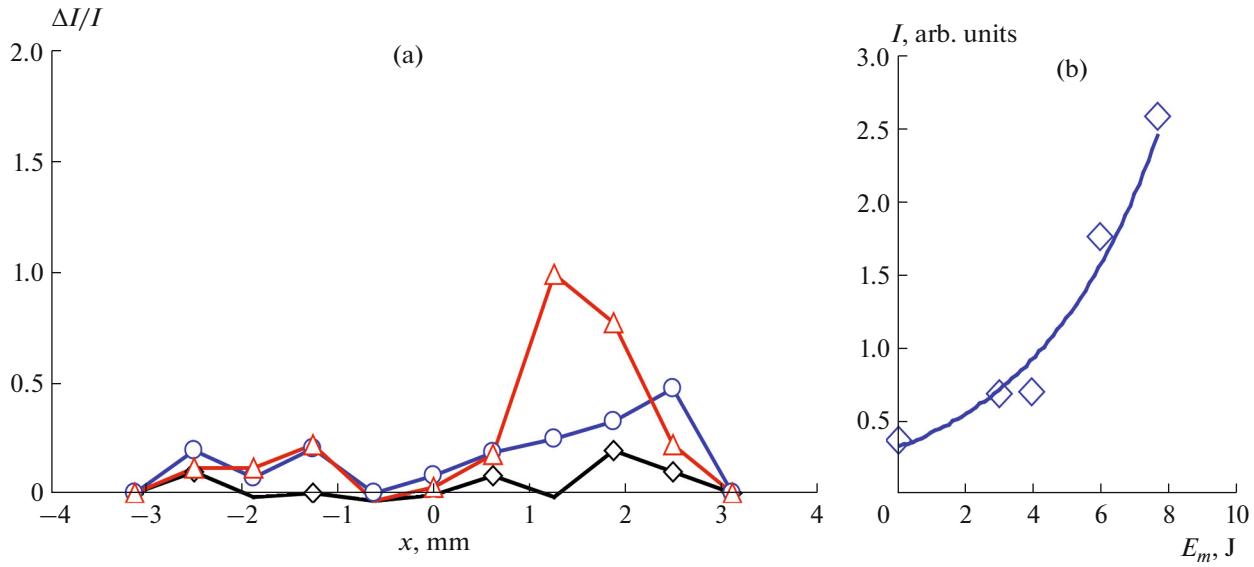

Fig. 5. (a) Normalized relative signal intensity profiles I on tomographic images of samples (◇, 2-16; ○, 2-9; △, 2-12) in the process of water absorption 260 days after the start; (b) dependence of the area integral under the normalized signal intensity profiles on the impact energy E_m.

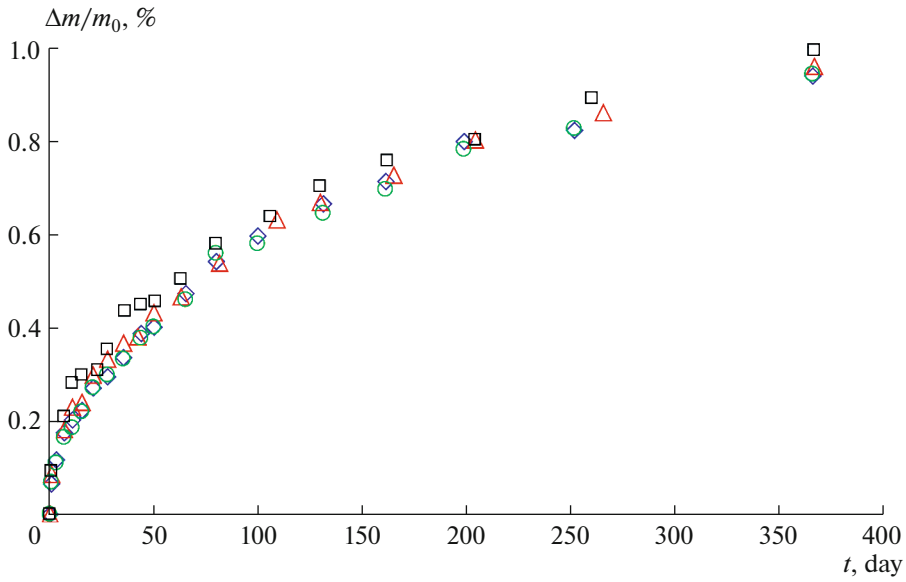

Fig. 6. Change in the mass of samples during exposure to water after cyclic alternating temperature impact: ◇, original sample; △, ○, □, correspond to 100, 350, and 1400 temperature cycles, respectively.

impact showed an almost complete absence of any influence of this effect on the quantitative nature of the change in the curves (Fig. 6). It is clearly seen that a reliably recorded difference is achieved only for a sample with the number of temperature cycles equal to 1400, while the absorption curves of the remaining samples coincide within the accuracy of the experiment. At the same time, the nature of moisture penetration itself does not change even with a large number of temperature cycles (1400)—only a slight increase in the total water absorption is observed. This effect is comparable in scale to the effect of a weak mechanical impact in cases where the integrity of the surface of the samples is preserved.

The tomographic images of samples during water absorption demonstrate a gradual increase in signal intensity from the near-surface regions (Fig. 7). It can be seen that the increase in signal intensity is symmet-

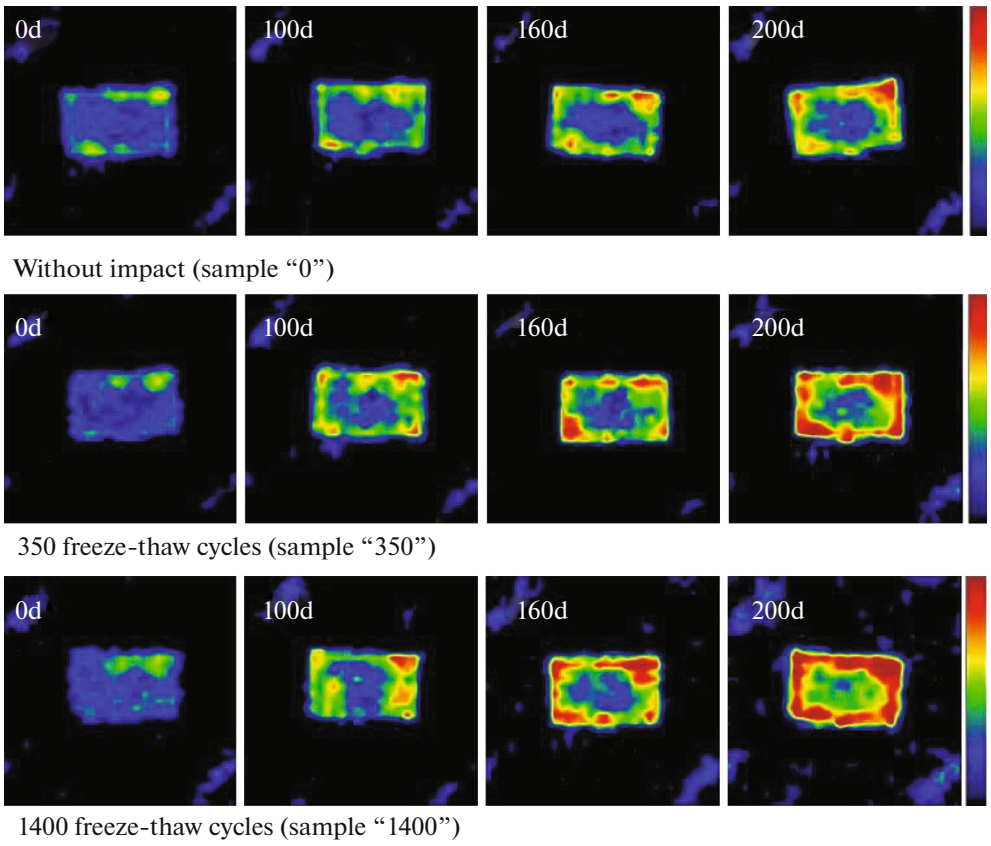

Fig. 7. Tomograms of control shots after water saturation of the original sample and samples after temperature alternating exposure.

rical; moreover, in the 1400 sample, the signal intensity in the tomograms is noticeably higher than in the control. This effect is also noticeable in signal intensity profiles plotted along the thickness of the sample. Thus, the difference between the last (200d) and initial (0d) profiles for the studied samples, normalized to the signal intensity of the initial profile (Fig. 8a), demonstrates symmetrical water absorption, in contrast to the impact-damaged samples. For the control and other samples, the increase in signal intensity is approximately the same from both planes, which indicates the absence of a preferential direction of diffusion and accumulation of water. However, in general, alternating temperature effects lead to the selective accumulation of water in the near-surface layers, which can be related to the accumulation of microscopic surface defects with an increase in the number of temperature cycles that promote water absorption in these areas.

Integration of the area under the presented curves showed that the relative increase in signal intensity linearly depends on the number of temperature cycles; however, on reaching ~500 cycles, the increase stops (Fig. 8b). Apparently, the number of accumulated defects reaches a maximum, and further alternating temperature cycling does not lead to the transition of their number to a new qualitative state (i.e., the formation of extended cracks, interlayer delaminations, etc.).

4. CONCLUSIONS

In this paper, the processes of water absorption by a PCM subjected to low-speed mechanical impact and alternating temperature cycling were studied. In addition to traditional weight measurements, this study used the MRI method to obtain information about the spatial distribution of the absorbed water in the material and the localization of areas of preferential water accumulation in it. The MRI method demonstrated that on samples after an impact (without visible damage), there is a predominant accumulation of moisture from a surface with a defective structure (on the opposite side from the impact). In the event of a violation of the integrity of the sample surface as a result of the impact, a significant accumulation of free water was found both directly in the area of destruction and in the adjacent layers to a depth of up to one-third of the sample's thickness. The MRI also shows that the moisture content in the PCM increases exponentially with increasing impact energy. This is due to the appearance of mechanical defects that provide free space that facilitates the penetration of water in the sample.

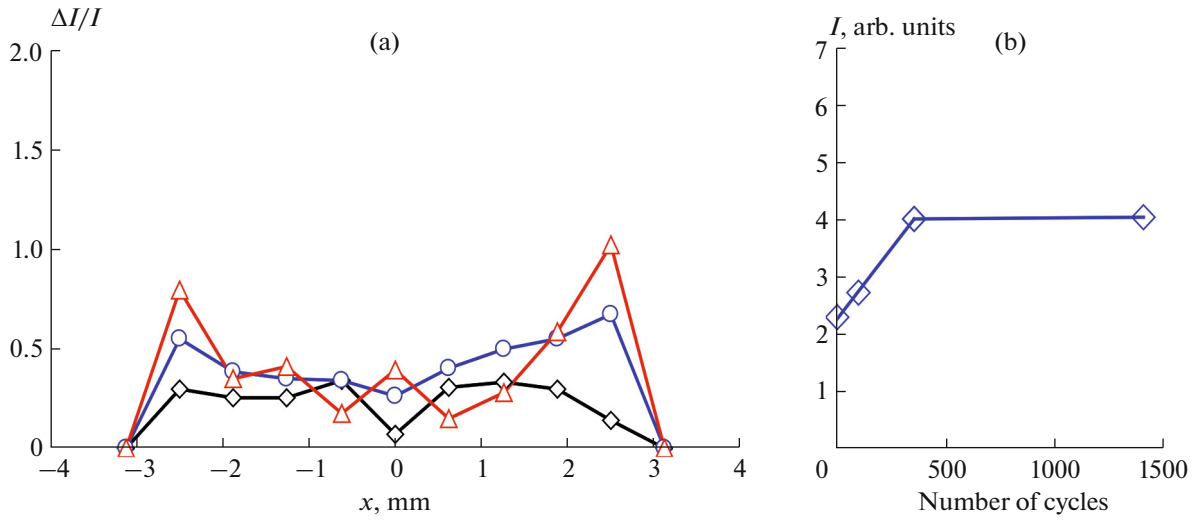

Fig. 8. (a) Normalized relative signal intensity profiles on tomographic images of samples (◇, 0; ○, 350; △, 1400) in the process of water absorption 200 days after the start; (b) dependence of the integral of the area under the normalized signal intensity profiles on the number of alternating temperature cycles.

It was found that cyclic alternating temperature impacts have a relatively weak effect on the amount of water absorbed by the samples. Only in the sample subjected to 1400 temperature cycles was a noticeable increase in the water content detected during long-term water absorption, which was caused by erosion due to the buildup of microdefects in the near-surface layers of the sample. The MRI method demonstrates a symmetrical picture of the localization of absorbed water in the near-surface layer of the sample, the amount of which increases linearly with the increase in the number of temperature cycles up to ~500, after which the growth stops.

The results obtained are important for predicting the behavior of PCMs under conditions of negative external influences, especially in the cases of the combined influence of factors such as mechanical shock and alternating temperature effects, complicated by the presence of water. The data obtained in the conducted studies showed the effectiveness of using the MRI method in diagnosing defects and mechanical damage to PCMs exposed to an humid environment.

ACKNOWLEDGMENTS

The research was carried out as part of a state assignment of the Institute of Chemistry and Chemical Technology of the Siberian Branch of the Russian Academy of Sciences (project no. 0287-2021-0012) using the equipment of the Krasnoyarsk Regional Center for Collective Use of the Federal Research Center "Krasnoyarsk Science Center of the Siberian Branch of the Russian Academy of Sciences."

FUNDING

This work was supported by ongoing institutional funding. No additional grants to carry out or direct this particular research were obtained.

CONFLICT OF INTEREST

The authors of this work declare that they have no conflicts of interest.

REFERENCES

1. M. L. Kerber, *Polymer Composite Materials. Structure. Properties. Technologies* (Professiya, St. Petersburg, 2008) [in Russian].
2. A. Y. Anpilova, E. E. Mastalygina, N. P. Khrameeva, et al., Russ. J. Phys. Chem. B **14**, 176 (2020). https://doi.org/10.1134/S1990793120010029
3. I. V. Klimenko, Russ. J. Phys. Chem. B **16**, 148 (2022). https://doi.org/10.1134/S1990793122010225
4. N. V. Korneeva, V. V. Kudinov, I. K. Krylov, et al., Russ. J. Phys. Chem. B **13**, 838 (2019). https://doi.org/10.1134/S1990793119050038
5. E. V. Nikolayev, M. R. Pavlov, A. B. Laptev, et al., Trudy VIAM. 56, 64 (2017). https://doi.org/10.18577/2307-6046-2017-0-8-7-7
6. Y. Wang, *Principles of Magnetic Resonance Imaging: Physics Concepts, Pulse Sequences, and Biomedical Applications* (CreateSpace Independent Publishing Platform, 2012), p. 374.
7. I. V. Koptyug, Prog. Nucl. Magn. Reson. Spectrosc. **65**, 1 (2012). https://doi.org/10.1016/j.pnmrs.2011.12.001
8. B. Blumich, *NMR Imaging of Materials* (Clarendon Press, 2003).

9. V. M. Bouznik, E. V. Morozov, I. A. Avilova, et al., Appl. Magn. Reson. **47**, 321 (2016). https://doi.org/10.1007/s00723-015-0748-2
10. E. V. Morozov, M. M. Novikov, and V. M. Bouznik, Addit. Manuf. **12**, 16 (2016). https://doi.org/10.1016/j.addma.2016.05.015
11. E. Morozov, M. Novikov, V. Bouznik, et al., Rapid Prototyp. J. **25**, 1007 (2019). https://doi.org/10.1108/RPJ-10-2018-0271
12. I. I. Sokolov and A. E. Raskutin, Trudy VIAM **4**, 4 (2013).
13. V. O. Startsev and A. V. Il'ichev, Mech. Compos. Mater. **54**, 145 (2018). https://doi.org/10.1007/s11029-018-9727-7
14. K. Berketis and D. Tzetzis, J. Mater. Sci. **45**, 5611 (2010). https://doi.org/10.1007/s10853-010-4626-x
15. V. O. Startsev, S. V. Panin, O. V. Startsev, Mech. Compos. Mater. **51**, 1081 (2015).
16. V. O. Startsev, A. Yu. Makhonkov, and E. A. Kotova, Aviat. Mater. Technol. **38**, 49 (2015). https://doi.org/10.18577/2071-9140-2015-0-S1-49-55
17. O. V. Startsev, K. O. Prokopenko, A. A. Litvinov, et al., Klei. Germetiki. Tekhnol. **8**, 18 (2009).
18. E. N. Kablov and O. V. Startsev, Aviat. Mater. Technol. **37**, 38 (2015). https://doi.org/10.18577/2071-9140-2015-0-4-38-52